

Optimized Parallel Joint Springs in Dynamic Motion: Comparison of Simulation and Experiment

Michael Scheint, Marion Sobotka, and Martin Buss

Abstract—Inspired by human tendon function, parallel springs in the joints of bipedal walking robots allow for a significant reduction of the cost of locomotion in simulation. An experimental setup is presented here which enables to verify the simulation results. The beneficial effects of parallel springs are investigated for a four-link robot arm equipped with a parallel spring at the last link. The desired motion results from simultaneous optimization of spring properties and motion which was shown to achieve the best reduction of actuation effort. Spring utilization is considered for two types of motion, free space motion and motion including contact with the environment at the end-effector. It is shown that the absolute reduction of effort through the utilization of an optimal spring is independent of friction. Hence, influence of the spring on effort is more relevant at higher speeds where the motion itself requires more actuation effort. Furthermore, for motion with environmental contact, a spring can reduce actuation effort more than in free space motion, especially for stiffer environments.

I. INTRODUCTION

Research activity toward the application of compliance in robotics especially bipedal walking robots or prosthetics has been motivated by the use of elasticity in the human muscle-tendon system. Fundamental possibilities of spring utilization are discussed in [1] with the aim of reducing actuator work by storing and releasing energy from springs. Optimal tuning of parallel and serial springs on a simulated human leg in [2] allows to replicate human leg torques during walking.

Leg prosthetics is one field which shows successful application of compliance. By adding springs to an ankle prosthesis [3], [4], necessary motor torques for walking can be considerably reduced allowing for smaller motors and batteries. Springs are also employed for gravity compensation of the arms of Willow Garage’s robot platform [5]. This allowed to use smaller motors and consequently made the arm backdriveable. Another possible application of springs is to increase peak output power or acceleration, as performed in [6] for the case of ball catching.

For the goal of making bipedal walking robots more efficient, springs reduce the required actuator input [7], [8], [9] substantially in simulations based on optimization of both walking motion and compliance. In [10], the simultaneous optimization of gait and a parallel ankle spring for a biped model not only leads to a more efficient gait but also to a more human-like gait. As in most simulations some simplifying modeling assumptions like neglecting friction are made, the open question is to what extent springs can reduce

actuation effort in a real hardware setup with non-neglectable friction introduced by the gears.

The main focus of this paper is to investigate the influence of a parallel spring on actuator effort in a hardware experiment with a robot arm and to examine the influence of modeling errors on spring exploitation. Since friction is one major disturbance that is usually neglected, optimal spring stiffness and optimal motion are obtained from minimizing actuation effort in simulation for both a model with approximated and one model without friction. Furthermore, spring usage is examined in two different motion types: free motion of a single link of the arm and whole arm motion with intermittent contact to the environment. The goal of this investigation is to help in the design of robotic systems which use springs for reduced actuator effort or higher peak power in a similar way as humans use tendons.

The remainder of the paper is structured as follows: Section II introduces the hardware setup and the considered scenarios in detail. In section III, the modeling, identification and compensation of friction on the employed robot arm is discussed. Section IV presents the optimization approach. In section V, optimization and experimental results are compared and discussed. Section VI contains the conclusion.

II. EXPERIMENTAL SETUP

For the experimental evaluation of the effects of springs on the actuation effort of a robotic device, the ViSHaRD4¹ device developed at our institute is used. It features four rigid links actuated by Maxon DC motors coupled through harmonic drive gears with a drive ratio of 100:1. Optical encoders are employed on each motor. The link axes of rotation are in parallel, resulting in a kinematically redundant arm, as shown in Fig. 1. The gears allow to amplify the motor torques but also introduce significant friction, which is discussed in the next section.

The complete dynamic model of the ViSHaRD4 arm with angular coordinates $\mathbf{q} = [q_1, q_2, q_3, q_4]^T$ (see Fig. 3) and its derivative $\dot{\mathbf{q}} = \frac{d}{dt}\mathbf{q}$ is derived using the Euler-Lagrange equation [11].

$$D(\mathbf{q})\ddot{\mathbf{q}} + C(\dot{\mathbf{q}}, \mathbf{q})\dot{\mathbf{q}} = \boldsymbol{\tau}_m - \boldsymbol{\tau}_f + \boldsymbol{\tau}_s + \mathbf{J}^T \mathbf{F} \quad (1)$$

Here, D denotes the inertia matrix, and $C\dot{\mathbf{q}}$ the matrix of Centrifugal- and Coriolis torques. There is no gravitational term, since the arm is parallel to the ground. The effective torque is composed of motor torque $\boldsymbol{\tau}_m$, friction torque $\boldsymbol{\tau}_f$,

All authors are with the Institute of Automatic Control Engineering, Technische Universität München, D-80290 München, Germany, {m.scheint, marion.sobotka}@tum.de, m.buss@ieee.org

¹Virtual Scenario Haptic Rendering Device



Fig. 1. Top view of the experimental setup. The ViSHaRD4 arm is shown together with the spring loaded plate.

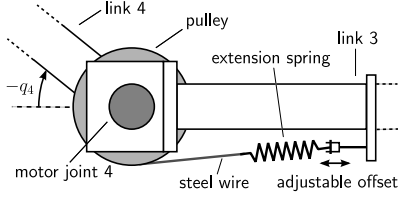


Fig. 2. Sketch of the spring attachment at joint 4 (not true to scale). The circular pulley is coupled to the output side of the gear.

spring torque τ_s , and torque due to forces \mathbf{F} at the end-effector. The model for the friction torque is described in the next section.

In order to investigate the effects of parallel springs, a linear extension spring is attached via a steel cable and a circular pulley to the last joint, as shown in Fig. 2. Although a spring at each joint is possible as well, we think that a single spring suffices to investigate the reduction of actuation effort by the spring. The second side of the spring is fixed to the previous link, with the offset being manually adjustable. The joint torque from the spring $\tau_{4,s}$ is piecewise linear.

$$\tau_{4,s} = \begin{cases} r_p^2 k_s (q_{s0} - q_4) + r_p F_{s,0} & \text{if } q_4 < q_{s0} \\ 0 & \text{otherwise} \end{cases} \quad (2)$$

Here, $r_p = 0.06\text{m}$ is the radius of the pulley, k_s the linear spring coefficient, F_0 the initial tension force of the spring, and q_{s0} the offset angle. A set of nine different springs is available for the experiments with stiffnesses ranging from $1.3 \frac{\text{kN}}{\text{m}}$ to $8.0 \frac{\text{kN}}{\text{m}}$, in approximately $1 \frac{\text{kN}}{\text{m}}$ steps.

Two different scenarios of arm motion are considered in this paper. For both cases, motion and spring stiffness are optimized simultaneously, once ignoring friction and once taking friction into account.

Scenario 1: A periodic motion of joint 4 is considered, with the joint required to move from $q_{4,0}$ to $q_{4,e}$ and back in a given time. This represents a point to point motion in free space as it occurs e.g. in pick & place operations.

Scenario 2: The complete arm performs a periodic motion with intermittent contact with the environment. The end-effector is required to approach a spring-loaded plate, move it along the y -axis only and return to the initial position as shown in Fig. 3. The force in y -direction is modeled as

$$F_p = \begin{cases} F_{p,0} + k_p (y_p - y) - F_{p,c} \text{sign}(\dot{y}) & \text{if } y < y_p \\ 0 & \text{otherwise} \end{cases} \quad (3)$$

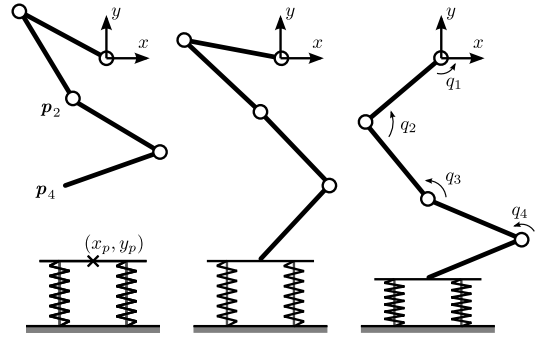


Fig. 3. Top view of scenario 2: Impact with spring loaded plate. First half of periodic motion is shown with top via point (left), contact point (center), and plate compression (right). The motion of the arm from first contact of the plate (center) until max. compression (right) is called *contact phase*.

with $k_p = 686 \frac{\text{N}}{\text{m}}$ and $F_{p,0} = 24\text{N}$. A set of via points and the cycle time specify this motion for later optimization. Motion with contact of the end-effector to the plate is referred to as *contact phase*, motion with no contact is called *free phase*. This scenario partially resembles the impact of a biped leg with the ground although it lacks the influence of gravity. A spring-loaded plate was chosen in favor of a rigid environment to avoid damages at the gear due to peak impact forces and to allow to investigate different environment stiffnesses.

III. FRICTION MODELING AND COMPENSATION

In the following, different friction phenomena are discussed and combined to a friction model for the ViSHaRD4 device. Then identification experiments are presented as well as details on the model-based compensation.

A. Friction Modeling

The friction of harmonic drives is affected by a variety of parameters including velocity, temperature, grease, applied load, and motor position. A detailed overview of friction phenomena and friction models is given e.g. in [12]. Commonly employed friction effects include Coulomb friction, a constant friction force opposite to the direction of motion, and stiction which describes friction at zero velocity. Viscous friction models the velocity dependence of friction with the standard linear model extended by a cubic term in [13]. Additional friction phenomena at low speed are included by the more elaborate dynamic LuGre model [14].

In the considered scenarios the fraction of low velocity is rather small, therefore LuGre model and stiction model are not used here. The chosen friction model here is a static velocity dependent friction map consisting of a direction dependent Coulomb friction term, and linear and cubic viscous terms.

$$\tau_{f,i} = \begin{cases} c_{i,0} + c_{i,2}\dot{q}_i + c_{i,3}\dot{q}_i^3 & \dot{q}_i > 0 \\ -c_{i,1} + c_{i,2}\dot{q}_i + c_{i,3}\dot{q}_i^3 & \dot{q}_i < 0 \end{cases} \quad (4)$$

The parameters $c_{i,j}$, $j \in [0, 1, 2, 3]$ of the friction model are estimated from an identification experiment for each joint i separately which is described next.

TABLE I
FRICTION IDENTIFICATION OF VISHARD4: SPEED RANGES AND
IDENTIFIED FRICTION PARAMETERS

link	$\dot{q}_{i,\max}$ in $\frac{\text{rad}}{\text{s}}$	c_1	c_2	c_3	c_4
1	[1, 2]	1.46	0.83	2.53	-0.21
2	[1, 2]	1.14	0.91	2.18	-0.19
3	[1, 2.5]	1.01	1.14	1.93	-0.12
4	[1, 3, 5]	1.72	1.05	1.14	-0.01

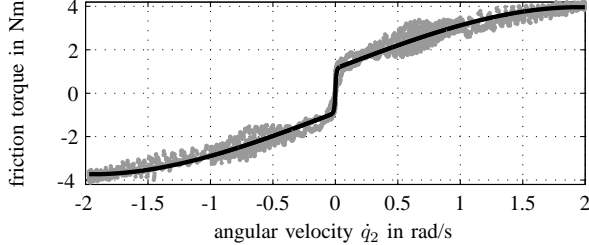


Fig. 4. Friction torque from identification experiment (gray) and estimated friction map (black line) for joint 2.

B. Friction Identification

For the estimation of the friction model parameters $c_{i,j}$, friction torque is calculated from desired and recorded motor torques at different speeds. In order to cover a desired speed range, each link is required to follow cosine trajectories with different maximum speeds.

$$q_i(t) = q_{i,0} + a(1 + \cos(\omega t)), \quad q_j(t) \equiv 0 \quad \forall j \neq i \quad (5)$$

$$\dot{q}_i \in [-\dot{q}_{i,\max}, \dot{q}_{i,\max}] \quad \text{with} \quad \dot{q}_{i,\max} = a\omega. \quad (6)$$

Here, q_i denotes the angle of the i -th link, a the amplitude, and ω the angular frequency of the cosine trajectory.

In the experiment, a PD controller together with the frictionless inverse system dynamics is used to track the desired trajectory. The maximum speeds $\dot{q}_{i,\max}$ for the individual links are shown in Table I together with the identified friction parameters. Parameters are fitted using a nonlinear least squares algorithm. The identified friction map together with the measurement data for joint 2 is shown in Fig. 4.

C. Friction Compensation

For the implementation of model-based friction compensation on the robot arm, the friction model (4) is extended by an exponential scaling around zero velocity as in [15] to avoid chattering behavior due to the noise of the differentiated position signal. Moreover, friction torque is additionally scaled to strictly underestimate friction.

$$\tau_{f,c,i} = c_u \tau_{f,i} \left(1 - e^{-c_e |\dot{q}_i|}\right) \quad (7)$$

Throughout the experiments the constants c_u, c_e are set to 0.92 and 150, respectively.

IV. TRAJECTORY OPTIMIZATION

For the aim of reducing actuator effort, simultaneous optimization of motion and spring properties has previously been shown to produce the best result [9]. A difficulty in motion optimization occurs in the contact phase, since the constrained end-effector motion results in a reduction of

degrees of freedom. For this purpose, the considered optimal control problem is first parameterized in the coordinate trajectories. The optimization in the contact phase is then possible by a special coordinate transformation. At the end of this section, a short discussion on the required torque for a frictionless single link motion shows the potential usefulness of springs and simultaneous optimization.

A. Parameterized Optimal Control Problem

The general optimal control problem for minimizing actuator effort is given by

$$\min_{\tau_m, k_s, q_{s0}} \int_0^T \|\tau_m(t)\|_2^2 dt \quad \text{s.t.} \quad \mathbf{n}_i \leq \mathbf{0}, \quad \mathbf{n}_e = \mathbf{0} \quad (8)$$

with a set of nonlinear inequality \mathbf{n}_i and equality \mathbf{n}_e constraints specifying the scenario and hardware limitations. In view of the second scenario which includes a phase with a kinematic constraint at the end-effector, the optimal control problem is parameterized by using Bezier polynomials of degree $M + 1$ for the desired joint trajectories \mathbf{q}_d .

$$\mathbf{q}_d(t) = \sum_{k=0}^M \alpha_k \binom{M}{k} (1-s)^{M-k} s^k, \quad s(t) = \frac{t-t_0}{t_1-t_0} \quad (9)$$

Here, s is a dimensionless path parameter defined using start time t_0 and final time t_1 of the considered motion. For given t_0, t_1 , joint motion is specified by the polynomial parameters $\alpha = [\alpha_0, \dots, \alpha_M]$. The corresponding motor torque τ_m is given by the inverse system dynamics.

$$\tau_m^* = D(\mathbf{q}_d) \ddot{\mathbf{q}}_d + C(\mathbf{q}_d, \dot{\mathbf{q}}_d) \dot{\mathbf{q}}_d + \tau_s(\mathbf{q}_d, k_s, q_{s0}) + \tau_f(\dot{\mathbf{q}}_d) \quad (10)$$

As the spring function (2) and the friction model (4) are known, the respective torques τ_s and τ_f are computed based on the desired trajectories.

By using (9) and (10), the original optimal control problem (8) is transformed to a parameterized optimal control problem, which is a nonlinear programming problem (NLP).

$$\min_{\alpha, k_s, q_{s0}} \int_T \|\tau_m(t, \alpha, k_s, q_{s0})\|_2^2 dt \quad (11)$$

$$\text{s.t.} \quad \mathbf{n}_i(t, \alpha, k_s, q_{s0}) \leq \mathbf{0}, \quad \mathbf{n}_e(t, \alpha, k_s, q_{s0}) = \mathbf{0}$$

This optimization problem is solved using the interior-point algorithm in MATLAB's `fmincon` solver. The desired trajectory is composed of several polynomials connected via continuity conditions on position and velocity. As only a finite number of springs are available for experiment, in the last step of optimization stiffness is fixed to the value of a real spring closest to the current optimized stiffness value.

B. Change of Coordinates during Contact Phase

In the second scenario, the end-effector contacts the spring-loaded plate and moves it along the spring axis only. For the world coordinate system as in Fig. 3, this is formulated as the following constraint on the end-effector position $\mathbf{p}_4 = [p_{4x}, p_{4y}]^T$.

$$p_{4x}(\mathbf{q}(t)) = x_p = \text{const.} \quad \text{if} \quad p_{4y} \leq y_p \quad (12)$$

In order to incorporate this constraint into optimization, the idea is, similar to the presented ones in [16], [17], to find a new set of minimal coordinates for the system under constraints and perform motion optimization in the new coordinates. The new coordinates w are chosen to contain the constrained variable p_{4x} and q_4 , the joint variable at the location of the spring.

$$w = [p_{4x} \quad p_{2y} \quad q_{3,abs} \quad q_4]^T = \varphi(q) \quad (13)$$

Here, p_{2y} is the y -position of the 2nd joint, $q_{3,abs}$ the absolute angle of the 3rd joint with respect to the world coordinate system. The coordinate transformation from q to w is completed by the following set of equations

$$\begin{aligned} \dot{w} &= J_w \dot{q}, \quad J_w = \frac{\partial \varphi}{\partial q}, \quad \det(J_w) = 0 \Leftrightarrow q_2 = 0 \\ \ddot{w} &= J_w \ddot{q} + \left(\frac{d}{dt} J_w\right) \dot{q} = J_w \ddot{q} + b_w \end{aligned} \quad (14)$$

with the transformation being valid for $q_2 \neq 0$ and the inverse transformation valid under certain bounds on p_{4x} and p_{2y} .

Based on the new coordinates w , the motor torque τ_m is obtained using the system dynamics (1) and above transformations (14).

$$\begin{aligned} \tau_m &= \tilde{D}(w) J_w^{-1} (\ddot{w} - b_w) + \tilde{C}(w, \dot{w}) J_w^{-1} \dot{w} \\ &\quad + \tau_s(w, k_s, q_{s0}) + \tilde{\tau}_f(\dot{w}) \end{aligned} \quad (15)$$

Using the coordinates w and equation (15), optimization for the contact phase can be accomplished by setting $w_1(t) \equiv x_{plate}$ and choosing Bezier polynomials for the remaining entries of w . Then, the optimal control problem is again parameterized as in (11) and can be solved similar to the unconstrained case.

V. RESULTS

In this section, the numerical simulation of the optimization results is compared to the experimental execution and analyzed with respect to spring utilization. The influence of friction and scenario on the achievable reduction of actuator effort is discussed. Four different cases are considered for each scenario in optimization:

- Case A: frictionless model, no spring considered
- Case B: frictionless model, spring optimized
- Case C: model with friction, no spring considered
- Case D: model with friction, spring optimized

This notation is combined with the scenario number, e.g. scenario 1 case A gives “1A”, in the following. In all experiments, the optimized trajectories are enforced by a PD controller with inverse dynamics and compensation for friction torque (4), spring torque (2) and torque from the spring-loaded plated (3) using model-based estimates.

A. Scenario 1 - Joint 4 Motion

The primary focus of scenario 1 is to examine the influence of friction on spring exploitation. Therefore, this scenario is optimized for different cycle times for the cases A-D, with the result considered in simulation and experiment.

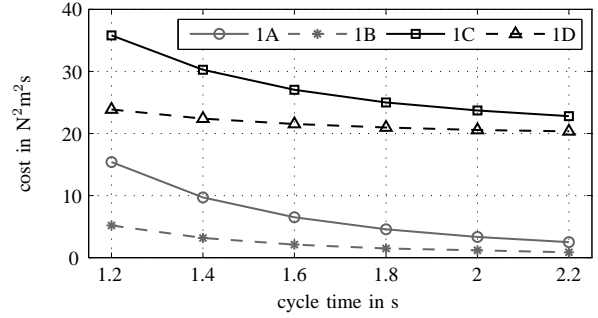


Fig. 5. Costs of different cases of scenario 1 over desired cycle time obtained from optimization. Solid lines represent optimization with no spring, dashed lines optimization with spring. A dark line indicates that friction was considered in optimization, light lines indicate a frictionless model. Nodes represent the actual data points

TABLE II

COSTS OF SCENARIO 1 IN EXPERIMENT AND SIMULATION IN N^2m^2s , EXPERIMENTAL DATA AVERAGED OVER 3 TRIALS

T	Data Source	Case 1A	Case 1B	Case 1C	Case 1D
1.2s	Simulation	15.4	5.2	35.8	23.8
	Experiment	31.5	22.2	36.4	25.9
	k_s in kN/m	–	7.9	–	7.9
2.0s	Simulation	3.3	1.2	23.7	20.5
	Experiment	23.0	20.2	22.6	20.8
	k_s in kN/m	–	5.9	–	5.1

1) *Optimization Results:* For optimization, the trajectory is composed of two Bezier polynomials of degree 10 connected at $q_{4,0} = 0$ and $q_{4,e} = \frac{\pi}{2}$. The numerical results are shown in Fig. 5 and Table II.

A comparison of the frictionless cases 1A and 1B shows that the cost reduction through using a spring is approximately constant for varying cycle time at approx. 66%. As expected, if friction is included in the system model, costs are generally higher. In cases 1C and 1D, relative cost savings from the spring are rather low at around 14% for a cycle time of $T = 2s$ but increase to 34% for $T = 1.2s$. But if the absolute cost savings from the optimized spring are considered, results for the frictionless case are similar to those from the case with friction. For a cycle time of $T = 1.2s$, the cost reduction through the spring is $10.2N^2m^2s$ for the cases 1A/1B, $12.0N^2m^2s$ for the cases 1C/1D. This observation holds for all cycle times as shown in Fig. 5.

From these results, it can be concluded that at low speeds the actuation necessary to overcome friction dominates the costs and therefore a spring can reduce costs only by a rather small percentage. For higher speeds, the actuation necessary to brake and re-accelerate the link becomes more dominant and allows to significantly reduce actuator effort by an optimally spring even in the presence of friction.

2) *Experimental Results:* The goal of the experiments is to verify whether the spring reduces actuator effort on real hardware as predicted in simulation despite remaining modeling errors and uncertainties. Optimization results of cases 1A to 1D for the cycle times $T = 1.2s$ and $T = 2.0s$ were executed on the hardware setup with the chosen

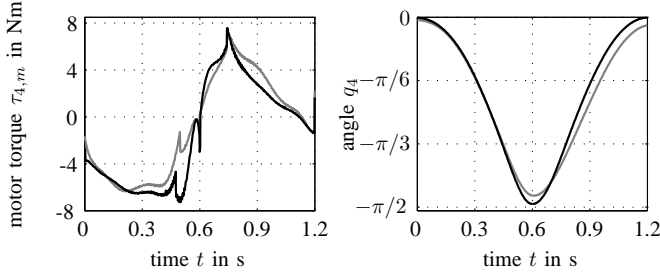


Fig. 6. Comparison of case 1B (gray line) and 1D (black line), showing commanded motor torque $u_{4,m}$ in the left plot and the angle q_4 over time in the right plot. Cycle time is 1.2s.

stiffness and spring offset. The results are summarized in Table II. In case of an optimization with the frictionless model (1A, 1B), the costs in the experiments are as expected higher due to friction. But the absolute difference between the costs with and without spring remain approximately similar for both cycle times. For the cases where friction is included in the model (1C/1D), experimental costs are close to those obtained from optimization.

A comparison with cases 1A and 1B shows that smaller costs are achieved in experiment if the trajectories from the frictionless optimization are used. A possible reason is that the identified friction model is imprecise due to temperature drift or unmodeled friction phenomena. The other explanation is based on the tracking error of cases 1A/1B. For those two cases, the PD controller has to cancel friction, leading to a tracking lag. As a result, the reversal point is earlier, e.g. for case 1B at the angle $q_{4,\min} = -1.48$ rad compared to $q_{4,\min} = -1.54$ rad for case 1D shown in Fig. 6.

In summary, the experimental results confirm the simulation findings when it comes to the achievable cost savings through spring utilization. Although the lowest costs are found if friction is not model-based compensated, this comes at the cost of a higher tracking error making a fair comparison difficult.

B. Scenario 2 - Motion with Environmental Contact

In this scenario spring exploitation is studied for motion with compression of the spring-loaded plate for two different plate stiffnesses. The hardware setup is shown in Fig. 1.

The desired trajectory is characterized by two waypoints for the end-effector, one for the apex and one for the point of maximum compression. For optimization, the trajectory is subdivided into 4 phases (see Fig. 3): apex to first contact (free phase), contact to max. compression (contact phase), max. compression to last contact (contact phase), and last contact to apex (free phase). In each phase, Bezier polynomials of degree 7 are used for each coordinate. The phase durations are fixed to 40% and 10% for free phases and contact phases, respectively. Numerical and experimental results for $T = \{1.2; 1.6; 2.0\}$ s are shown in Table III.

1) *Optimization Results:* The comparison of costs over cycle times shows that for the softer plate stiffness, costs decrease with rising cycle time. For the stiffer plate however, the medium cycle time has the lowest costs, the plate eigenfrequency obviously better fitting the fixed phase times.

TABLE III
COSTS OF SCENARIO 2 IN EXPERIMENT AND SIMULATION IN $\text{N}^2\text{m}^2\text{s}$,
EXPERIMENTAL DATA AVERAGED OVER 3 TRIALS

T	Data Source	$k_p = 0.6 \frac{\text{kN}}{\text{m}}$		$k_p = 1.3 \frac{\text{kN}}{\text{m}}$	
		Case 2C	Case 2D	Case 2C	Case 2D
1.2s	Simulation	149.1	137.0	142.7	125.4
	Experiment	179.4	167.5	162.3	148.4
	k_s in kN/m	–	5.1	–	5.9
1.6s	Simulation	107.3	93.8	119.1	84.0
	Experiment	130.3	111.3	139.6	94.5
	k_s in kN/m	–	5.9	–	7.1
2.0s	Simulation	93.8	85.0	136.6	85.9
	Experiment	111.9	100.4	146.0	104.2
	k_s in kN/m	–	5.9	–	7.9

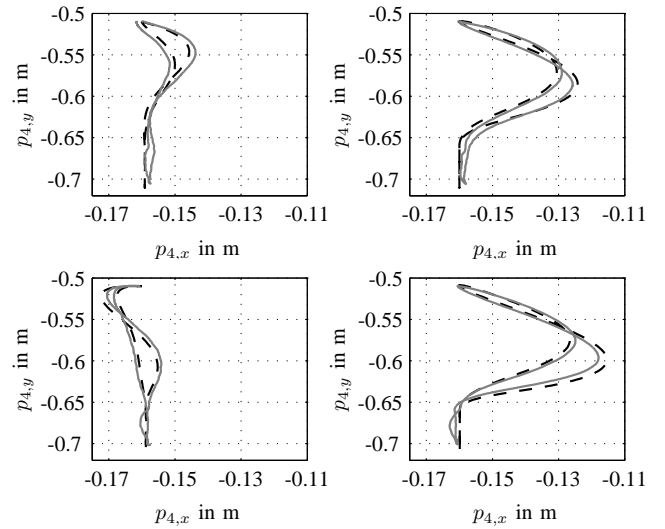


Fig. 7. End-effector trajectory $p_4(t)$ in x - y plane for the plate with spring stiffness of $0.6 \frac{\text{kN}}{\text{m}}$ (top) and $1.3 \frac{\text{kN}}{\text{m}}$ (bottom row), both at a cycle time of 1.6s, optimization result (dashed) and experimental result (solid). On the left side, case 2C is shown, on the right side case 2D.

For the softer plate, the spring in joint 4 can reduce actuation effort by a rather low amount with a maximal reduction of $13.5 \text{N}^2\text{m}^2\text{s}$ for $T = 1.6\text{s}$. A larger reduction of effort is obtained from the spring for the harder plate, with a maximal reduction of $35.1 \text{N}^2\text{m}^2\text{s}$ at $T = 1.6\text{s}$. The latter reduction is larger since the stiffer plate requires more actuation at joint 4, with the costs evaluated for total torque being $50.2 \text{N}^2\text{m}^2\text{s}$ compared to $25.6 \text{N}^2\text{m}^2\text{s}$ for the soft plate.

2) *Experimental Results:* The experimentally determined costs shown in Table III confirm the results from optimization with respect to reduction of actuation effort through the spring. Absolute costs are higher than in simulation, which can be traced back to modeling errors e.g. through unmodeled viscous friction at the plate. But since the main interest lies in cost differences between the respective cases, this additional cost offset is not important.

Apart from modeling errors, tracking errors also influence costs. A suitable measure for the tracking behavior is the obtained maximum compression of the plate with the desired value being 5.0cm. For case 2D and a cycle time of $T = 1.6\text{s}$,

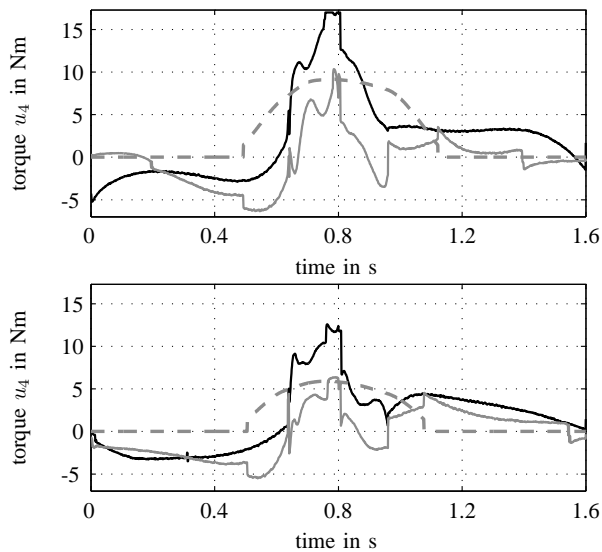


Fig. 8. Torques at joint 4 in experiment for the plate with spring stiffness of $0.6 \frac{\text{kN}}{\text{m}}$ (top) and $1.3 \frac{\text{kN}}{\text{m}}$ (bottom). Motor torque $u_{4,m}$ for case 2C is indicated with a black line, for case 2D $u_{4,m}$ with a gray solid line. Spring torque $u_{4,s}$ of case 2D is shown in gray dashed.

this value is about 4.5cm for the soft plate and about 4.1cm for the stiff plate. Since higher compression results in higher peak forces and hence, higher torques, this clearly affects the costs. However, tracking error is mostly dependent on plate stiffness and cycle time, leaving the primary goal, verification of spring influence, untouched.

Another interesting observation is that independent of cycle time, the optimally chosen spring reduces actuation effort at link 4 to comparable remaining costs of about 13 to $16 \text{N}^2 \text{m}^2 \text{s}$. Obviously there exists a lower bound for the remaining actuation at joint 4 due to friction, acceleration/deceleration at apex, and other.

3) *Discussion*: Summarizing the results for scenario 2, both simulation and experiment showed the trend that at higher environment stiffness a higher reduction of actuation effort can be achieved as higher torques are required at joint 4. Although total costs are reduced for the soft plate already, the reduction is more significant for the stiffer plate. In contrast to scenario 1, cost reduction through the spring does not necessarily increase for higher speed, i.e. lower cycle time.

VI. CONCLUSIONS

Optimization of motion and stiffness was presented for the 4-link robot arm ViSHARD4 with a parallel spring at the last joint. A friction model was identified and used for optimization and model-based compensation in experiments. Optimization was performed using a parameterized optimal control problem suitable for unconstrained and kinematically constrained motion. Two different scenarios were considered. It was shown for a single link motion that friction has only a small influence on the absolute cost reduction achieved through spring utilization. At higher speeds, the cost reduction from the spring becomes more significant compared to actuation costs related to friction. For motion

with environmental contact, a larger cost reduction through the spring is possible, especially for a stiffer environment but with less dependence on speed of motion. In summary, this paper supports the simulation based findings for using springs in bipedal walking. Even in the presence of friction, springs can significantly reduce actuation effort and increase peak torque, making parallel springs a viable option for bio-inspired robotic devices.

ACKNOWLEDGMENTS

This work was supported in part within the Grant WO1440/2-1 of the German Research Foundation (DFG).

REFERENCES

- [1] R. M. Alexander, "Three uses for springs in legged locomotion," *The International Journal of Robotics Research*, vol. 9, no. 2, pp. 53–61, 1990.
- [2] K. Endo and H. Herr, "A model of muscle-tendon function in human walking," in *Proceedings of the IEEE International Conference on Robotics and Automation (ICRA)*, 2009, pp. 1909–1915.
- [3] S. Au and H. Herr, "Powered ankle-foot prosthesis," *Robotics & Automation Magazine, IEEE*, vol. 15, no. 3, pp. 52–59, 2008.
- [4] R. Bellman, M. Holgate, and T. Sugar, "Sparky 3: Design of an active robotic ankle prosthesis with two actuated degrees of freedom using regenerative kinetics," in *Proceedings of the IEEE International Conference on Biomedical Robotics and Biomechanics (BioRob)*, 2008, pp. 511–516.
- [5] K. Wyrobek, E. Berger, H. Van der Loos, and J. Salisbury, "Towards a personal robotics development platform: Rationale and design of an intrinsically safe personal robot," in *Proceedings of the IEEE International Conference on Robotics and Automation (ICRA)*, 2008, pp. 2165–2170.
- [6] M. Kaneko, M. Higashimori, R. Takenaka, A. Namiki, and M. Ishikawa, "The 100 g capturing robot - too fast to see," *IEEE/ASME Transactions on Mechatronics*, vol. 8, no. 1, pp. 37–44, 2003.
- [7] V. Duindam and S. Stramigioli, "Optimization of mass and stiffness distribution for efficient bipedal walking," in *Proceedings of the International Symposium on Nonlinear Theory and its Applications*, Bruges, Belgium, 2005.
- [8] K. Mombaur, "Using optimization to create self-stable human-like running," *Robotica*, vol. 27, no. 03, pp. 321–330, 2009.
- [9] M. Scheint, M. Sobotka, and M. Buss, "Compliance in gait synthesis: Effects on energy and gait," in *Proceedings of the IEEE International Conference on Humanoid Robots*, Daejeon, Korea, 2008, pp. 259–264.
- [10] T. Schaub, M. Scheint, M. Sobotka, and M. Buss, "Effects of compliant ankles on bipedal locomotion," in *Proceedings of the IEEE International Conference on Robotics and Automation (ICRA)*, Kobe, Japan, 2009, pp. 2761–2766.
- [11] M. W. Spong and M. Vidyasagar, *Robot Dynamics and Control*. New York, NY, USA: John Wiley & Sons, Inc., 1989.
- [12] M.-W. Ueberle, "Design, control, and evaluation of a family of kinesthetic haptic interfaces," Ph.D. dissertation, Technical University of Munich, 2006.
- [13] T. Tuttle and W. Seering, "A nonlinear model of a harmonic drive gear transmission," *IEEE Transactions on Robotics and Automation*, vol. 12, no. 3, pp. 368–374, jun 1996.
- [14] C. Canudas de Wit, H. Olsson, K. Astrom, and P. Lischinsky, "A new model for control of systems with friction," *IEEE Transactions on Automatic Control*, vol. 40, no. 3, pp. 419–425, 1995.
- [15] J.-P. Hauschild and G. Heppler, "Control of harmonic drive motor actuated flexible linkages," in *Proceedings of the IEEE International Conference on Robotics and Automation (ICRA)*, 2007, pp. 3451–3456.
- [16] M. Scheint, M. Sobotka, and M. Buss, "Virtual holonomic constraint approach for planar bipedal walking robots extended to double support," in *Proceedings of the IEEE International Conference on Decision and Control (CDC)*, 2009, pp. 8180–8185.
- [17] S. Miossec, K. Yokoi, and A. Kheddar, "A method for trajectory optimization of robots having contacts or motion constraints," in *Proceedings of the IEEE Conference on Robotics, Automation and Mechatronics*, 2006, pp. 1–6.